ACS OMEGA

Article

Cite This: ACS Omega 2018, 3, 4105−4112

Impact of Oxygen Functional Groups on Reduced Graphene Oxide-Based Sensors for Ammonia and Toluene Detection at Room Temperature

Cherukutty Ramakrishnan Minitha,[†] Velunair Sukumaran Anithaa,[‡] Vijayakumar Subramaniam,[§] and Ramasamy Thangavelu Rajendra Kumar*[,†,∥]

[†]Advanced Materials and Devices Laboratory (AMDL), Department of Physics, [‡]Department of Physics, [§]Department of Medical Physics, and [∥]Department of Nanoscience and Technology, Bharathiar University, Coimbatore 641 046, India

Supporting Information

ABSTRACT: The chemically reduced graphene oxide (rGO) was prepared by the reduction of graphene oxide by hydrazine hydrate. By varying the reduction time (10 min, 1 h, and 15 h), oxygen functional groups on rGO were tremendously controlled and they were named RG1, RG2, and RG3, respectively. Here, we investigate the impact of oxygen functional groups on the detection of ammonia and toluene at room temperature. Their effect on sensing mechanism was analyzed by first-principles calculation-based density functional theory. The sensing material was fabricated, and the effect of reduction time shown improved the recovery of ammonia and toluene sensing at room temperature. Structural, morphological, and electrical characterizations were performed on both RG1 and RG3. The sensor response toward toluene vapor of 300 ppm was found to vary 4.4, 2.5, and 3.8% for RG1, RG2, and RG3, respectively. Though RG1 shows higher sensing response with poor recovery, RG3 exhibited complete desorption of toluene after the sensing process with response and recovery times of approximately 40 and 75 s, respectively. The complete recovery of toluene molecules on RG3 is due to the generation of new sites after the reduction of oxygen functionalities on its surface. It could be suggested that these sites provided anchor to ammonia and toluene molecules and good recovery under N_2 purge. Both theoretical and experimental studies revealed that tuning the oxygen functional groups on rGO could play a vital role in the detection of volatile organic compounds (VOCs) on rGO sheets and was discussed in detail. This study could provoke knowledge about rGO-based sensor dependency with oxygen functional groups and shed light on effective monitoring of VOCs under ambient conditions for air quality monitoring applications.

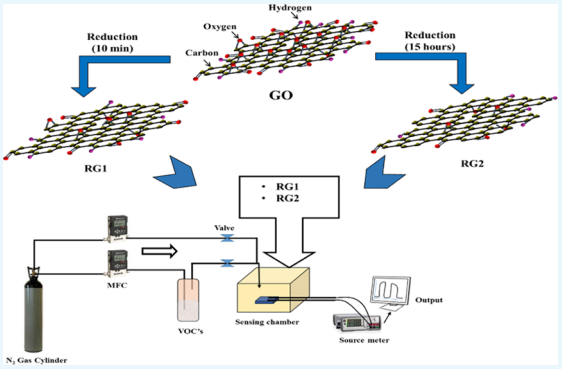

1. INTRODUCTION

The industries such as automotive, oil, chemical, and plastic have mandated the usage of gas monitors which could be advantageous if they could be available as a reliable handheld battery-operated device.[1] Nowadays, ammonia and toluene are the most common indoor air pollutants and harmful to human health which are increasing in earth's atmosphere along with greenhouse gases (carbon dioxide, methane, water vapor, and nitrous oxide).[2] Toluene is used in the preparation of paints, metal cleaners, plastics, detergents, and indispensable cancer biomarkers.[3,4] Ammonia has emerged as an indoor atmosphere pollutant which appears mainly due to the hydrolysis of urea which exists in the antifreeze additives in concrete buildings.[5] There has been an increased demand to develop a cost-effective, portable, and highly sensitive device under ambient conditions, which is still a challenging task to the scientific community. Some spectrometry techniques such as photo-ionization and ion mobility were used to measure the trace detection of volatile organic compounds (VOC), and they are limited because of their equipment cost and prior sample preparation.[4] For the last two decades, metal oxides such as CeO_2, SnO_2, WO_3, silicon nanowire, and metal oxide framework have been used for sensing VOCs, chemical warfare agents, and explosive gases.[3,6−10] Nonetheless, these metal oxide-based sensing materials require high operating temperature and power which complicate the sensing performance.[11]

Carbon-based nanomaterials have exciting properties of high surface area and electron transport under ambient conditions which are the promising candidate for portable sensors.[12,13] Carbon nanotubes,[14] fullerenes,[15] and carbon-based composites[16] were widely demonstrated as ambient condition sensor materials. Recently, a new generation of toxic gas sensing materials was demonstrated using two-dimensional nanostructures like graphene-based materials.[17−19] The reduced graphene

Received: December 29, 2017
Accepted: April 4, 2018
Published: April 12, 2018

DOI: 10.1021/acsomega.7b02085
ACS Omega 2018, 3, 4105−4112

oxide (rGO) consists of oxygen functional groups partially decorated on the graphene sheets with $\pi-\pi$ bonds and defect [missing of carbon atom in its series (i.e., holes)][19] sites which act as active sites to the analyte molecules. Therefore, rGO-based sensing materials have become a potential competitor for the above-mentioned materials.

In this paper, the effect of oxygen functional groups in chemically rGO on ammonia and toluene molecules was studied. We found that rGO is highly activated by surface functionalities such as carboxyl, epoxy functional groups, and $\pi-\pi$ interaction for physical and chemical adsorption for these gas molecules. It was revealed that the reduction time of graphene oxide (GO) can be tuned to get better response and complete recovery of the sensor. The response of the sensor was carried out in the presence of ammonia/toluene, and nitrogen (N_2) was used as a carrier gas for room-temperature gas sensing measurements. First-principles calculation of density functional theory (DFT) was also executed to understand the role of oxygen functionalities on rGO toward sensing mechanisms.

2. RESULTS AND DISCUSSION

Figure 1a–c shows the field emission scanning electron microscopy (FESEM) image of rGO, which confirmed the graphene sheet morphology, and it was observed to be crumpled. $I-V$ characteristics of rGO for different reduction times of 10 min (RG1), 1 h (RG2), and 15 h (RG3) are shown in Figure 1d. The applied voltage ranged from −5 to +5 V. The linear $I-V$ plot confirms good ohmic contact between the sensing materials and Ag electrodes. The resistance of rGO gradually decreases with increasing reduction time from 10 min to 15 h (~2.2 MΩ to 5.4 KΩ).

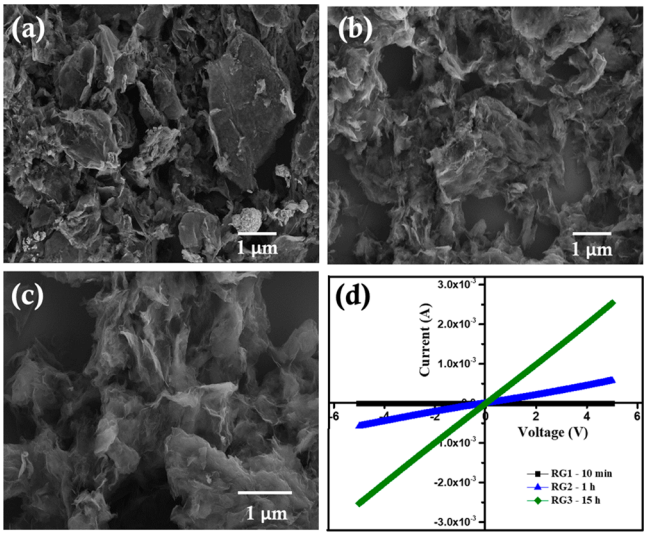

Figure 1. FESEM images of (a) RG1 (10 min), (b) RG2 (1 h), and (c) RG3 (15 h). The scale bar is 1 μm. (d) $I-V$ characteristics of the RG1, RG2, and RG3 coated on a Ag electrode.

To observe the variation in oxygen functional groups, rGO was characterized by X-ray diffraction (XRD), Fourier transform infrared (FTIR), and Raman measurement (Figure 2). From Figure 2a, it was revealed that upon oxidation of graphite flakes, the (002) plane at 26.5° was shifted to (001) at 10.5° with complete intercalation of oxygen functionalities.[20] By the reduction of GO, the (001) plane shifted from 14.2° to 24.1° for 10 min (RG1) and 24.19° for 15 h (RG3). It was confirmed that in the case RG1, there was only a partial reduction occurring during 10 min, and for RG3, the (002) plane resorted to graphite nature at 15 h. It was observed that RG1 and RG3 have a diffraction peak at 43.1°, which could be attributed to short-range ordering in stacked graphene layers.[21] Figure 2b shows the FTIR spectra of GO, RG1, and RG3. The band at 1565 cm^{-1} was assigned to C═C stretching of sp^2 carbon atoms. The shift in the C═C band was due to restoration of the π-network because of the elimination of oxygen functional groups[22,23] in the reduction process. The vibrations at 1413 and 1182–1022 cm^{-1} were assigned to deformation vibrations of C–OH groups and C–O–C or ketones, respectively.[20] The bands at 1724 cm^{-1} for GO and 1632 cm^{-1} for RG1 and RG3 were attributed to the asymmetric vibrations of carboxylic groups. The shift of C═O revealed that with the reduction time, oxygen functional groups were decreased.[20,22,24] The increase in the reduction time of GO is clearly shown by the decrease in the intensity of the band at 1632 cm^{-1} (–COOH) groups. The structural analysis of RG2 (1 h) was discussed in Supporting Information Figure S1.

From Raman spectra (Figure 2c), the I_D/I_G ratio of RG1 (1.05) and RG3 (1.07) has increased notably with that of GO (1.02). This indicates that the reduction time altered the structure of GO.[20,25]

The change in the electrical response of sensing materials for ammonia/toluene (300 ppm) under 35% relative humidity (% RH) is shown in Figure 3. It was observed that the resistance of the sensor increased while introducing analytes. As anticipated, all five cycles have consistency for analyte gases. From Figure 3a,b, RG1 having higher oxygen functionalities shows good response for toluene (100 second—ON) than ammonia (very poor response) and it did not completely recover to the initial resistance upon carrier gas purge (100 second—ON). It could be suggested that the adsorbed toluene molecules do not desorb completely during recovery process. Because of this behavior of RG1, the response of the sensor decreases upon consecutive ON and OFF cycles of vapor injection. Similarly, for RG2, the recovery was poor upon each consecutive cycles (Figure 3a). This indicates that the presence of functional groups might facilitate chemisorption of ammonia molecules.[26,27] Therefore, it shows poor recovery under N_2 purge. In RG3, after recovery, it retained its base resistance on N_2 purge (100 s). This suggested that the removal of oxygen functional groups might facilitate for the complete recovery of the analyte. The stability of the RG3 sensor was tested with 10 consecutive cycles under 40% RH. The sensor shows the repeatability and stability of both analytes (Figure S2a,b, respectively).

The response of the sensor was calculated using eqs 2 and 3. It is one of the key parameters to describe the efficiency of sensing materials to gas or vapor. For the RG3 sensor, the response toward 300 ppm of toluene was found to be 3.8% and, for ammonia, was 3.1%. In this study, the response of the sensors (RG1, RG2, and RG3) was tested for both the analytes, ammonia and toluene, in different RHs (30–80%) and is presented in Figures S3 and S4. It was observed that there is an influence of humidity to the response of the sensor for both the analytes, ammonia and toluene. In the case of ammonia, the sensor (RG2) shows poor recovery in the presence of humidity, whereas in RG3, there is partial recovery. For toluene, it was observed that with an increase in reduction, there is a complete recovery, which further shows an increase with the increase in

DOI: 10.1021/acsomega.7b02085
ACS Omega 2018, 3, 4105–4112

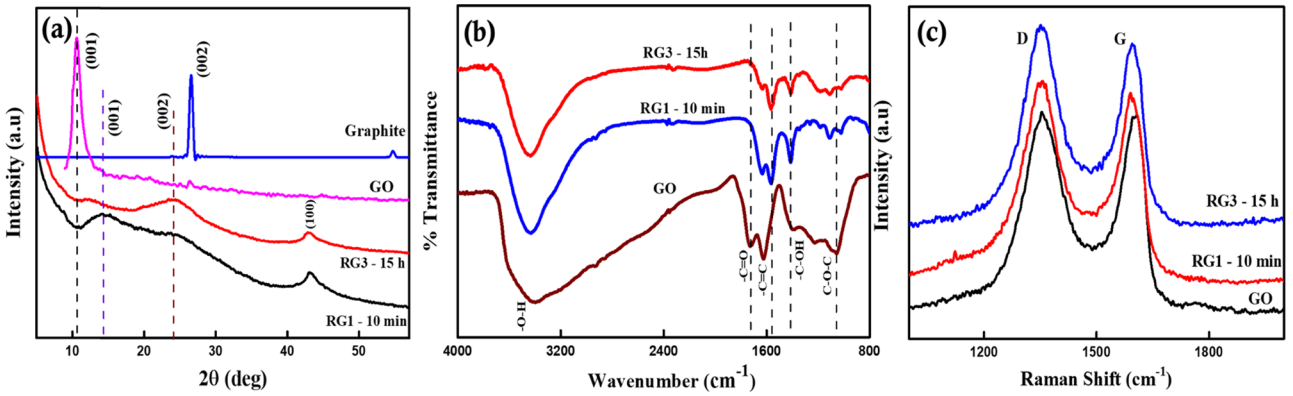

Figure 2. (a) XRD, (b) FTIR, and (c) Raman spectra of RG1 and RG3. The graphite and GO peaks were used as a reference. The bands/peaks are labeled.

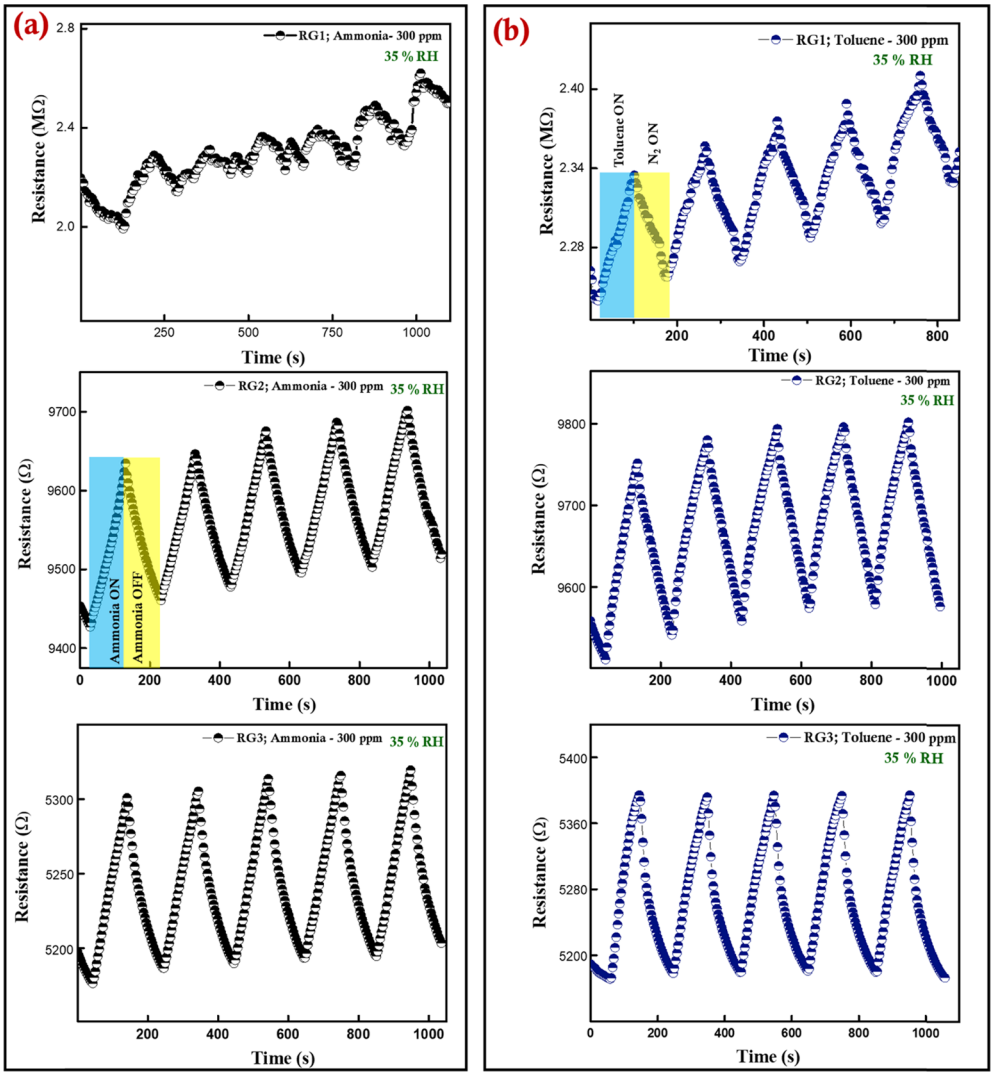

Figure 3. Electrical response of rGO-based sensors (RG1, RG2, and RG3) as a function of time for the detection of 300 ppm (a) ammonia and (b) toluene for five consecutive cycles under 35% relative humidity.

humidity. From this, it was believed that humidity could influence the response and recovery of the sensor.

Figure 4a shows the RG3 sensor response to toluene at different concentrations (100−2800 ppm). It was observed that sensor response increased with an increase in the analyte concentration. The calculated response of the sensor was 2.9% at 100 ppm to 7.8% at 3000 ppm for toluene. The response of the sensor devices varied linearly with the concentration (Figure 4b). The regression coefficient values for ammonia and toluene were 0.9890 and 0.9932, respectively.

Figure 5a shows the sensor response of RG3 toward 300 ppm of toluene and other VOCs. Ammonia and toluene

DOI: 10.1021/acsomega.7b02085
ACS Omega 2018, 3, 4105−4112

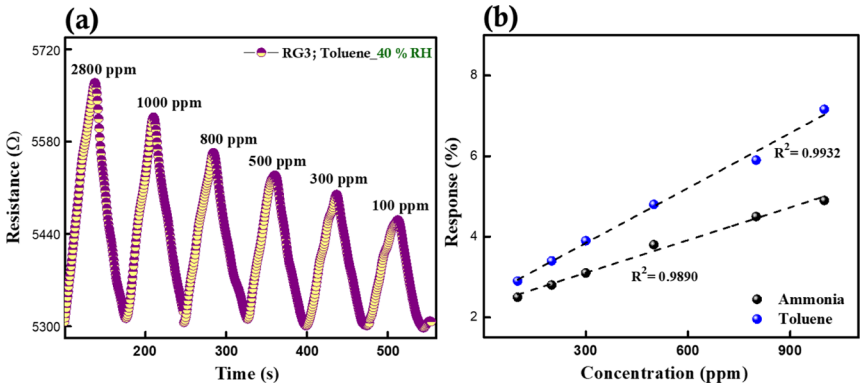

Figure 4. (a) Response of the RG3 sensor to toluene in different concentrations (100−2800 ppm) and (b) linear fit of sensor response vs ammonia/toluene concentrations (100−1000 ppm).

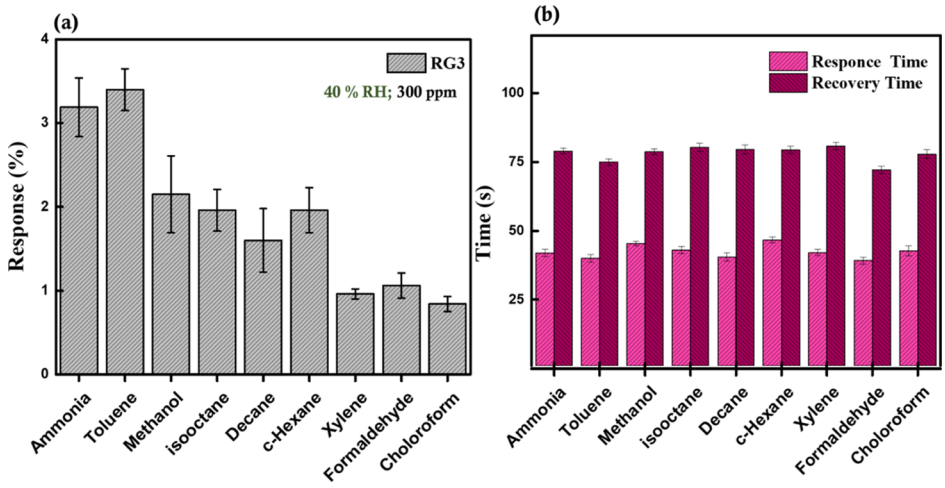

Figure 5. (a) Sensor response of the RG3 sensor to different gases at room temperature under 40% RH and (b) response and recovery times of the RG3 sensor to 300 ppm test gases at room temperatures.

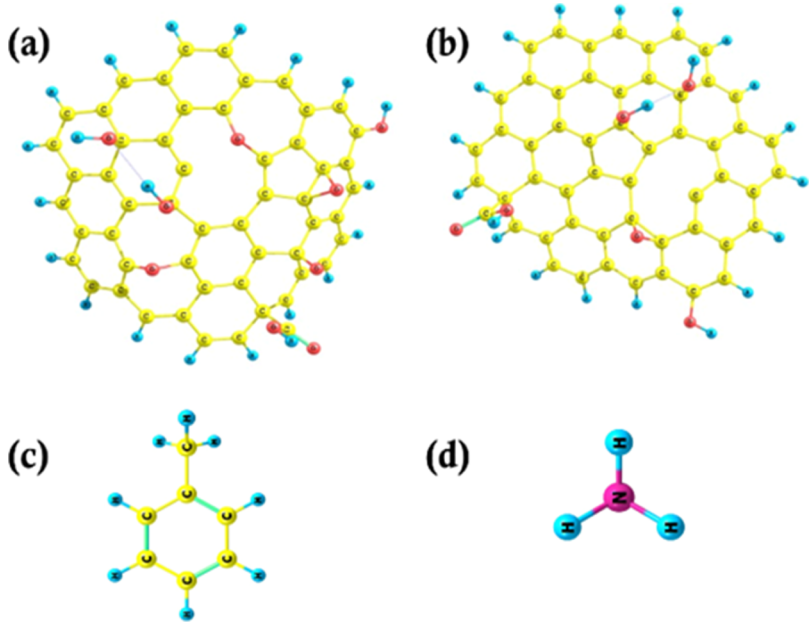

Figure 6. (a) Top view of the optimized molecular structure of (a) $RG1_{(s)}$ and (b) $RG3_{(s)}$. Optimized molecular structures of (c) toluene and (d) ammonia molecules.

DOI: 10.1021/acsomega.7b02085
ACS Omega 2018, 3, 4105−4112

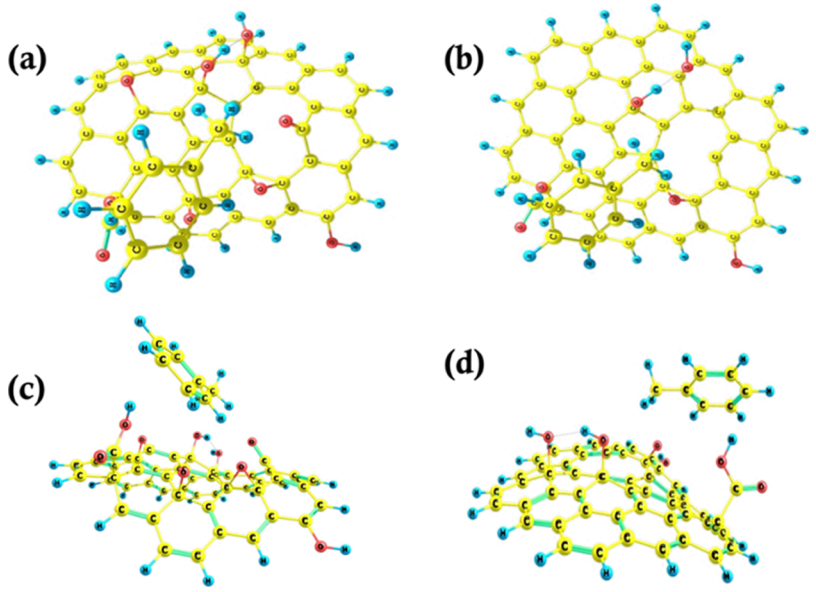

Figure 7. Optimized molecular structure of toluene interacted on $RG1_{(s)}$ (a,c) and (b,d) $RG3_{(s)}$.

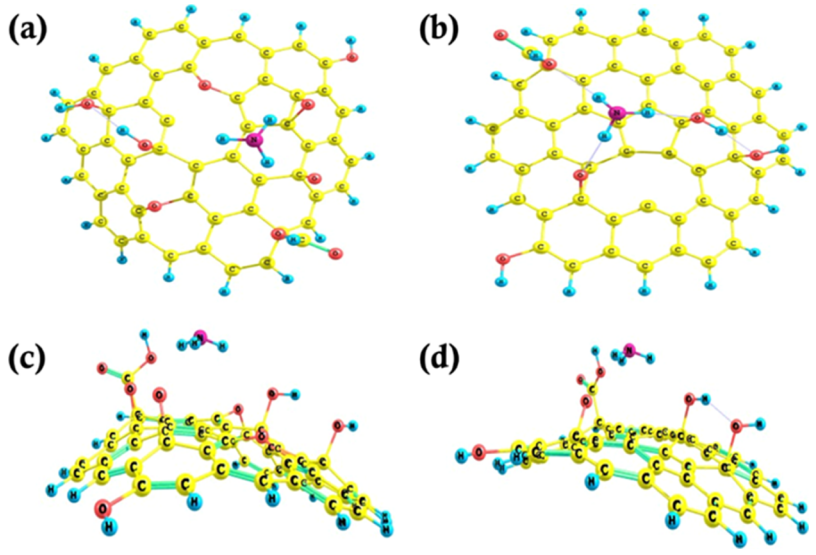

Figure 8. Optimized molecular structure of ammonia interacted on $RG1_{(s)}$ (a,c) and (b,d) $RG3_{(s)}$.

showed higher sensor response than other gases, and corresponding response and recovery times are shown in Figure 5b. The calculated response and recovery times for toluene were approximately 40 and 75 s, respectively. The sample was responded to all tested VOCs and did not show specific selectivity. Further tuning of surface-active sites of the sensor materials is to be done to improve the selectivity.

The response times of analyte molecules were 45 s for RG1 and 40 s for RG3, whereas the recovery times were 83 s for RG1 and 75 s for RG3. It could be noted that RG1 has a baseline drift which could be mainly attributed to the uncompleted desorption of analyte molecules.[1] Upon repeated test cycles, more residual analyte molecules existed in the sensor materials. It was not removed by the carrier gas within 100 s to achieve an initial base resistance. It could be suggested that excess of oxygen functional groups presence on the surface of RG1 could cause good response toward the analyte, but it was difficult to completely desorb within a fixed cycle period. From FTIR spectra (Figure 2b), it was clear that the presence of carboxylic, epoxy, and hydroxyl groups on the surface of rGO was gradually removed with the increase in the reduction time (10 min to 15 h). The reduction by hydrazine hydrate (N_2H_4) raises the reduction-based defects, reorganization of sp^2 carbon ($\pi-\pi$ interactions), and residual oxygen functional groups on the basal plane. The optimized amount of these active sites could enhance the sensor's performance. In this case, it is suggested that more physisorption takes place, enabling a faster recovery within 100 s for RG3 than RG1. However, the response time was faster in the case of RG1 with higher oxygen functional groups. The charge transfers between analytes and rGO sensor were discussed in few reports.[19,26] Understanding the role of oxygen functional groups on response and favorable interaction sites is still an open challenge.

To understand the interaction of the ammonia and toluene gas molecules on the RG1 and RG3 sheets, DFT was used. The optimized molecular structure of the two different kinds of rGO sheet ($RG1_{(s)}$ and $RG3_{(s)}$) is shown in Figure 6a,b, respectively. In the rGO sheet, three unsaturated carbon atoms are

DOI: 10.1021/acsomega.7b02085
ACS Omega 2018, 3, 4105−4112

rearranged to form a nine-membered ring adjacent to a pentagon. The epoxy group was preset at the dangling bond site and also in the other possible sites along with −COOH and −OH functional groups. Additionally, the hydrogen atoms were passivated in the remaining unsaturated carbon edges. The optimized structures of toluene and ammonia (monomer) gas molecules are presented in Figure 6c,d, respectively.

The gas molecules were adsorbed on the rGO sheet over a monovacancy defect with parallel orientation of toluene and ammonia facing the pentagon of the rGO sheet which is shown in Figures 7 and 8, respectively. From the results, it was confirmed that the binding energy of toluene (1.56 eV) was higher than that of ammonia (0.260 eV) with $RG1_{(s)}$ and this binding energy is found to decrease further for both toluene (0.042 eV) and ammonia (0.040 eV) with $RG3_{(s)}$. The high binding energy of toluene was due to the electron-donating ability of the methyl group attached to the benzene ring which induces charge transfer from toluene to rGO, whereas the charge gain in ammonia without the dissociation of N−H bond shows the charge transfer from rGO to ammonia. The calculated nearest adsorption distance, adsorption energy (E_{ads}) of gas molecules on the rGO surface, Mulliken charges (MC), and the energy gap E_g are tabulated in Table 1. Thus, from the above results, it was confirmed that the ammonia gas molecule has less affinity than the toluene molecule to the rGO sheets.

Table 1. Binding Energy and Nearest Distance (Å), MCs, and Band Gap for the Monomers and the rGO Complex[a]

complex	adsorption height (Å)	adsorption energy (eV)	MC (e)	band gap E_g (eV)
RG3				1.229
RG3-NH_3	3.4	−0.040	−0.915 (−0.888)	1.270
RG3-C_7H_8	4.6	−0.042	−0.515 (−0.529)	1.335
RG1				1.507
RG1-NH_3	3.4	−0.260	−0.893 (−0.888)	1.284
RG1-C_7H_8	4.2	−1.567	−0.508 (−0.529)	1.477

[a]The values represented in bracket correspond to the MCs of monomer.

With the adsorption energy values, the recovery time was calculated using conventional transition-state theory, where the recovery time τ was expressed as

$$\tau = \upsilon_0^{-1}\, e^{(-E_{ads}/K_B T)} \quad (1)$$

where T is the temperature, K_B is Boltzmann's constant, and and υ_0 is the attempt frequency. From this equation, it was found that increasing the adsorption energy E_{ads} will enhance the recovery time; the strong interaction makes the desorption to be harder and implies longer recovery time. From the results, the adsorption energies were short which illustrates the short recovery time. Together with the experimental results, we can conclude that the high number of oxygen atoms increases the adsorption of toluene and ammonia. Further, the epoxy and hydroxyl groups on the basal plane satisfy the dangling bond in the defect, giving rise to lesser binding energy of ammonia.

From both experimental and theoretical results, it was confirmed that the binding energy of toluene/ammonia with RG1 is higher compared to that of RG3. Because of this nature, RG1 shows poor desorption than RG3 (Figure 3). From this, it was suggested that the controlled reduction of oxygen functional groups on rGO could increase the performance of the sensors.

3. CONCLUSIONS

The rGO-based sensing materials were fabricated on a Ag electrode by the drop-casting method. The difference in sensing response and recovery of ammonia/toluene vapor at room temperature was studied. The results revealed that higher oxygen functional groups functionalized on the rGO surface yield higher sensor response and poor recovery, whereas moderate sensing response with complete desorption was obtained in less oxygen-functionalized rGO. It was believed that humidity could influence the response of the sensor. It was revealed that controlled reduction of GO shows good response for ammonia and toluene. Furthermore, because of room-temperature operation, this kind of VOC sensors with controlled oxygen functional groups on the surface of rGO could be promising for environmental and industrial applications.

4. EXPERIMENTAL SECTION

4.1. Preparation of rGO. rGO was prepared from chemical reduction of GO using our previous reported procedure.[28] In brief, hydrazine hydrate (1 mL) was added into the dispersed GO solution. The solution was heated in an oil bath at 100 °C with a water-cooled condenser for 10 min (RG1), 1 h (RG2), and 15 h (RG3); during this reaction time, reduced GO gradually precipitated out as a black solid. The product was isolated by vacuum filtration, washed copiously with water and methanol, and finally dried at 60 °C.

4.2. Fabrication of a Sensor. The sensor device was fabricated by drop-casting the rGO dispersion onto silver electrodes. The Ag electrodes were fabricated using thermal evaporation on a glass substrate. rGO (10 μL, 0.5 mg/1 mL) was drop-casted on Ag electrodes and then dried at 60 °C. Further annealing was carried out at 80 °C for 10 h in a hot air oven to remove excess water molecules and improve contacts between rGO and Ag electrodes. The sensor device was placed in a chamber with an electrical feedthrough. A constant voltage of +0.5 V was applied to the device. The variation in resistance was monitored and recorded with the changes in the atmospheric environment (ammonia/toluene analytes and N_2 gas) using an Agilent B2902A source meter. The sensing measurement cycle is as follows: first, N_2 atmosphere (1000 sccm) was introduced as the carrier gas, and then, an analyte gas (20−100 sccm) was injected to record the sensing signal and again N_2 gas was introduced for sensor recovery. The change in resistance (ΔR) and the response of the sensor was calculated[1] as given by eqs 2 and 3

$$\Delta R = R_{analyte} - R_{N_2} \quad (2)$$

$$\text{Sensor response}\ (\%) = \frac{\Delta R}{R_b} \times 100 \quad (3)$$

where R_{N_2} is the resistance of rGO in a N_2 atmosphere and $R_{analyte}$ is the resistance of rGO in the presence of ammonia/toluene vapor (ohms). R_b is the base resistance of the sensing material in ohms. The relative atmospheric humidity was 35%. The RH was adjusted from 30 to 80% to measure the influence of humidity on the response of the sensor.

DOI: 10.1021/acsomega.7b02085
ACS Omega 2018, 3, 4105−4112

4.3. Computational Details. A rGO sheet of approximately 19 benzene rings with the reconstructed monovacancy defect and the functional groups such as −COOH, −OH, and −C−O groups distributed on the basal, edges, and at defects sites, respectively, was constructed. Further, rGO sheets of high and low number of oxygen atoms were considered as $C_{55}H_{21}O_9$ and $C_{55}H_{21}O_6$ with C/O ratios of 13:1 and 6:1 in relation with the experimental data and named $RG1_{(s)}$ (simulated rGO) and $RG3_{(s)}$, respectively. The interaction of ammonia and toluene gas molecules on the surface of rGO was optimized using DFT. The B3LYP function values of electronic properties are similar to the experimental values,[29] as the 6-31G* basis function is commonly used for physisorption in carbon nanomaterials[30,31] and it suited well for the present work. The frequency calculations were carried out for all optimized structures to confirm their minima on the potential energy surface. All of the calculations were executed using the Gaussian 09[32] software package. The adsorption energy of the gas molecules (ammonia—NH_3 and toluene—C_6H_5–CH_3) was calculated using eq 4

$$E_{ads} = E_{rGO} + NH_3 - (E_{NH_3} + E_{rGO}) \quad (4)$$

where E_{rGO+NH_3}, E_{NH_3}, and E_{rGO} are the total energies of the NH_3 gas molecule-adsorbed rGO complex, monomer NH_3 gas molecule, and the bare rGO sheet, respectively. Similar calculation is carried out for the toluene gas molecule by replacing the energy of toluene instead of ammonia.

4.4. Instruments and Characterizations. The XRD pattern of the as prepared rGO was investigated by a Bruker ADVANCE D8 instrument. The morphology was examined by FESEM (FEI—QUANTA—FEG 250). Raman spectroscopy was performed on a Raman microscope (HORIBA Jobin Yvon, HR800) with an excitation wavelength of 514 nm. The optical analysis was performed with an optical microscope (Olympus BX51P). The current−voltage characterization and sensing measurement were performed using an Agilent B2902A source meter.

■ ASSOCIATED CONTENT

Supporting Information

The Supporting Information is available free of charge on the ACS Publications website at DOI: 10.1021/acsomega.7b02085.

XRD and FTIR spectra of RG2; stability of the RG3 sensor with 10 repetitive cycles in the presence of 40% RH toluene and ammonia; response of the rGO-based sensor for the detection of 300 ppm of ammonia at different RHs; and response of the rGO-based sensor for the detection of 300 ppm of toluene at different RHs (PDF)

■ AUTHOR INFORMATION

Corresponding Author

*E-mail: rtrkumar@buc.edu.in. Phone : +91-9789757888 (R.T.R.K.).

ORCID

Ramasamy Thangavelu Rajendra Kumar: 0000-0002-4188-5859

Notes

The authors declare no competing financial interest.

■ ACKNOWLEDGMENTS

The authors C.R.M. and R.T.R.K. would like to thank the Department of Science and Technology, Government of India, for financial support under the SERB project (SR/FTP/PS-099/2011). C.R.M. would like to thank DST—PURSE, New Delhi, India for providing FESEM facility.

■ REFERENCES

(1) Ghosh, R.; Midya, A.; Santra, S.; Ray, S. K.; Guha, P. K. Chemically reduced graphene oxide for ammonia detection at room temperature. *ACS Appl. Mater. Interfaces* **2013**, *5*, 7599−7603.

(2) Assen, A. H.; Yassine, O.; Shekhah, O.; Eddaoudi, M.; Salama, K. N. MOFs for the Sensitive Detection of Ammonia: Deployment of fcu-MOF Thin-Films as Effective Chemical Capacitive Sensors. *ACS Sens.* **2017**, *2*, 1294.

(3) Gregis, G.; Schaefer, S.; Sanchez, J.-B.; Fierro, V.; Berger, F.; Bezverkhyy, I.; Weber, G.; Bellat, J.-P.; Celzard, A. Characterization of materials toward toluene traces detection for air quality monitoring and lung cancer diagnosis. *Mater. Chem. Phys.* **2017**, *192*, 374−382.

(4) Li, Z.; Xu, C.; Shu, J. Detection of sub-pptv benzene, toluene, and ethylbenzene via low-pressure photoionization mass spectrometry. *Anal. Chim. Acta* **2017**, *964*, 134−141.

(5) Zhang, D.; Liu, J.; Jiang, C.; Liu, A.; Xia, B. Quantitative detection of formaldehyde and ammonia gas via metal oxide-modified graphene-based sensor array combining with neural network model. *Sens. Actuators, B* **2017**, *240*, 55−65.

(6) Kida, T.; Nishiyama, A.; Hua, Z.; Suematsu, K.; Yuasa, M.; Shimanoe, K. WO3 nanolamella gas sensor: porosity control using SnO2 nanoparticles for enhanced NO2 sensing. *Langmuir* **2014**, *30*, 2571−2579.

(7) Sui, L.; Zhang, X.; Cheng, X.; Wang, P.; Xu, Y.; Gao, S.; Zhao, H.; Huo, L. Au-Loaded Hierarchical MoO3 Hollow Spheres with Enhanced Gas-Sensing Performance for the Detection of BTX (Benzene, Toluene, And Xylene) And the Sensing Mechanism. *ACS Appl. Mater. Interfaces* **2017**, *9*, 1661−1670.

(8) Ueda, T.; Abe, H.; Kamada, K.; Bishop, S. R.; Tuller, H. L.; Hyodo, T.; Shimizu, Y. Enhanced sensing response of solid-electrolyte gas sensors to toluene: Role of composite Au/metal oxide sensing electrode. *Sens. Actuators, B* **2017**, *252*, 268.

(9) Plonka, A. M.; Wang, Q.; Gordon, W. O.; Balboa, A.; Troya, D.; Guo, W.; Sharp, C. H.; Senanayake, S. D.; Morris, J. R.; Hill, C. L. In Situ Probes of Capture and Decomposition of Chemical Warfare Agent Simulants by Zr-Based Metal Organic Frameworks. *J. Am. Chem. Soc.* **2017**, *139*, 599−602.

(10) Paska, Y.; Stelzner, T.; Christiansen, S.; Haick, H. Enhanced sensing of nonpolar volatile organic compounds by silicon nanowire field effect transistors. *ACS Nano* **2011**, *5*, 5620−5626.

(11) Zhou, Y.; Jiang, Y.; Xie, G.; Du, X.; Tai, H. Gas sensors based on multiple-walled carbon nanotubes-polyethylene oxide films for toluene vapor detection. *Sens. Actuators, B* **2014**, *191*, 24−30.

(12) Georgakilas, V.; Perman, J. A.; Tucek, J.; Zboril, R. Broad family of carbon nanoallotropes: classification, chemistry, and applications of fullerenes, carbon dots, nanotubes, graphene, nanodiamonds, and combined superstructures. *Chem. Rev.* **2015**, *115*, 4744−4822.

(13) Jariwala, D.; Sangwan, V. K.; Lauhon, L. J.; Marks, T. J.; Hersam, M. C. Carbon nanomaterials for electronics, optoelectronics, photovoltaics, and sensing. *Chem. Soc. Rev.* **2013**, *42*, 2824−2860.

(14) Kumar, D.; Chaturvedi, P.; Saho, P.; Jha, P.; Chouksey, A.; Lal, M.; Rawat, J. S.B.S.; Tandon, R. P.; Chaudhury, P. K. Effect of single wall carbon nanotube networks on gas sensor response and detection limit. *Sens. Actuators, B* **2017**, *240*, 1134−1140.

(15) Yong, Y.; Lv, S.; Zhang, R.; Zhou, Q.; Su, X.; Li, T.; Cui, H. C 54 Si 6 heterofullerene as a potential gas sensor for CO, NO, and HCN detection. *RSC Adv.* **2016**, *6*, 89080−89088.

(16) Travlou, N. A.; Bandosz, T. J. Nanoporous carbon-composites as gas sensors: Importance of the specific adsorption forces for ammonia sensing mechanism. *Carbon* **2017**, *121*, 114.

DOI: 10.1021/acsomega.7b02085
ACS Omega 2018, 3, 4105−4112

(17) Schedin, F.; Geim, A. K.; Morozov, S. V.; Hill, E. W.; Blake, P.; Katsnelson, M. I.; Novoselov, K. S. Detection of individual gas molecules adsorbed on graphene. *Nat. Mater.* **2007**, *6*, 652−655.
(18) Some, S.; Xu, Y.; Kim, Y.; Yoon, Y.; Qin, H.; Kulkarni, A.; Kim, T.; Lee, H. Highly sensitive and selective gas sensor using hydrophilic and hydrophobic graphenes. *Sci. Rep.* **2013**, *3*, 1868.
(19) Cui, S.; Pu, H.; Mattson, E. C.; Wen, Z.; Chang, J.; Hou, Y.; Hirschmugl, C. J.; Chen, J. Ultrasensitive chemical sensing through facile tuning defects and functional groups in reduced graphene oxide. *Anal. Chem.* **2014**, *86*, 7516−7522.
(20) Minitha, C. R.; Lalitha, M.; Jeyachandran, Y. L.; Senthilkumar, L.; Rajendra Kumar, R. T. Adsorption behaviour of reduced graphene oxide towards cationic and anionic dyes: Co-action of electrostatic and $\pi-\pi$ interactions. *Mater. Chem. Phys.* **2017**, *194*, 243−252.
(21) Stobinski, L.; Lesiak, B.; Malolepszy, A.; Mazurkiewicz, M.; Mierzwa, B.; Zemek, J.; Jiricek, P.; Bieloshapka, I. Graphene oxide and reduced graphene oxide studied by the XRD, TEM and electron spectroscopy methods. *J. Electron Spectrosc. Relat. Phenom.* **2014**, *195*, 145−154.
(22) Acik, M.; Lee, G.; Mattevi, C.; Pirkle, A.; Wallace, R. M.; Chhowalla, M.; Cho, K.; Chabal, Y. The role of oxygen during thermal reduction of graphene oxide studied by infrared absorption spectroscopy. *J. Phys. Chem. C* **2011**, *115*, 19761−19781.
(23) Pavia, D. L.; Lampman, G. M.; Kriz, G. S.; Vyvyan, J. A. *Introduction to Spectroscopy*; Cengage Learning, 2008.
(24) Manickam, S.; Muthoosamy, K.; Bai, R. G.; Abubakar, I. B.; Sudheer, S. M.; Hongngee, L.; Hwei-San, L.; Nayming, H.; Ch, C. Exceedingly biocompatible and thin-layered reduced graphene oxide nanosheets using an eco-friendly mushroom extract strategy. *Int. J. Nanomed.* **2015**, *10*, 1505.
(25) Pimenta, M.; Dresselhaus, G.; Dresselhaus, M. S.; Cançado, L. G.; Jorio, A.; Saito, R. Studying disorder in graphite-based systems by Raman spectroscopy. *Phys. Chem. Chem. Phys.* **2007**, *9*, 1276−1290.
(26) Tang, S.; Cao, Z. Adsorption and dissociation of ammonia on graphene oxides: a first-principles study. *J. Phys. Chem. C* **2012**, *116*, 8778−8791.
(27) Peng, Y.; Li, J. Ammonia adsorption on graphene and graphene oxide: a first-principles study. *Front. Environ. Sci. Eng.* **2013**, *7*, 403−411.
(28) Minitha, C. R.; Rajendrakumar, R. T. Synthesis and characterization of reduced graphene oxide. *Adv. Mater. Res.* **2013**, *678*, 56−60.
(29) Banerjee, S.; Bhattacharyya, D. Electronic properties of nanographene sheets calculated using quantum chemical DFT. *Comput. Mater. Sci.* **2008**, *44*, 41−45.
(30) Tachikawa, H.; Iyama, T. Structures and electronic states of fluorinated graphene. *Solid State Sci.* **2014**, *28*, 41−46.
(31) Umadevi, D.; Sastry, G. N. Feasibility of carbon nanomaterials as gas sensors: a computational study. *Curr. Sci.* **2014**, *106*, 1224.
(32) Frisch, M.; Trucks, G.; Schlegel, H.; Scuseria, G.; Robb, M.; Cheeseman, J.; Scalmani, G.; Barone, V.; Mennucci, B.; Petersson, G. *Gaussian 09*, Revision A.1., Program for Quantum Chemical Calculations; Gaussian Inc.: Wallingford, CT, 2009.

DOI: 10.1021/acsomega.7b02085
ACS Omega 2018, 3, 4105−4112